



# Identification of the dehydration active sites in glycerol hydrogenolysis to 1,2-propanediol over Cu/SiO<sub>2</sub> catalysts



Jianfeng Shan<sup>a,b,c,1</sup>, Huan Liu<sup>a,c,1</sup>, Kuan Lu<sup>a,c,d</sup>, Shanhui Zhu<sup>a,\*</sup>, Junfen Li<sup>a</sup>, Jianguo Wang<sup>a,c</sup>, Weibin Fan<sup>a,\*</sup>

<sup>a</sup> State Key Laboratory of Coal Conversion, Institute of Coal Chemistry, Chinese Academy of Sciences, 27 South Taoyuan Road, Taiyuan 030001, People's Republic of China

<sup>b</sup> College of Chemistry and Material Science, Shandong Agricultural University, 61 Daizong Road, Tai'an 271018, People's Republic of China

<sup>c</sup> University of Chinese Academy of Sciences, Beijing 100049, People's Republic of China

<sup>d</sup> National Energy Center for Coal to Clean Fuels, Synfuels China Co., Huairou District, Beijing 101400, People's Republic of China

## ARTICLE INFO

### Article history:

Received 30 July 2019

Revised 18 December 2019

Accepted 18 December 2019

### Keywords:

Glycerol  
Hydrogenolysis  
1,2-Propanediol  
Cu/SBA-15  
Interface

## ABSTRACT

Metal–support interaction is a hot topic in catalysis, but attention has seldom been drawn to the promotional effect of metal–irreducible SiO<sub>2</sub> interfaces. Here, Cu/SBA-15 catalysts with Cu–O–Si–O– interface structures were prepared by simple grinding, and showed high activity and selectivity to 1,2-propanediol above 97% in liquid-phase glycerol hydrogenolysis. Glycerol conversion of ground Cu/SBA-15 with 10% Cu loading was about seven times that of its impregnation counterpart. The linear relationship between turnover frequency and (Cu–O–Si–O– induced Lewis acid sites)/Cu<sup>0</sup> ratio indicated that Cu–O–Si–O– structures were crucial for achieving excellent hydrogenolysis performance. More importantly, in situ Fourier transform infrared spectroscopy of glycerol adsorption and density functional theory calculation results confirmed that Cu–O–Si–O– species were the dominant active dehydration sites of glycerol hydrogenolysis, while the adjacent Cu sites were involved in subsequent hydrogenation of the generated hydroxyacetone.

© 2019 Elsevier Inc. All rights reserved.

## 1. Introduction

Utilization of biomass-derived feedstock provides a way to reduce consumption of diminishing fuel and benefit the global climate by reducing greenhouse gas emissions [1,2]. Recently, biodiesel has emerged as a promising substitute for conventional fossil fuels. It is well known that glycerol accounts for approximately 10 wt% of the total product in the biodiesel process. Although the production of glycerol is growing rapidly, its market condition is poor [3–5]. Therefore, transformation of glycerol into value-added products is highly desirable for increasing profits in the biodiesel industry. 1,2-Propanediol (1,2-PDO) is widely used in the synthesis of unsaturated polyester resins, pharmaceuticals, cosmetics, and so on [6,7]. Currently, 1,2-PDO is produced from propylene oxide that comes from selective oxidation of petroleum-derived propylene. Thus, the hydrogenolysis of glycerol to 1,2-PDO is a promising route for saving fossil fuel and upgrading glycerol utilization.

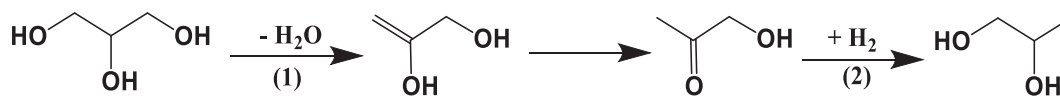
During the past decade, the hydrogenolysis of glycerol to 1,2-PDO over different metal catalysts (e.g., Pt, Ru, Ag, Rh, Ir, Cu, Co

and Ni) has been studied extensively [2,5,8–21]. Among them, copper-based catalysts have been demonstrated to be the best candidates for their poor ability to cleave C–C bonds, while giving excellent 1,2-PDO selectivity [3,6,22]. Various metallic/nonmetallic oxides, such as chromite, Al<sub>2</sub>O<sub>3</sub>, MgO, MgAlO, AlOOH, ZrO<sub>2</sub>, ZnO, and SiO<sub>2</sub>, have been employed as supports for Cu-based catalysts for hydrogenolysis of glycerol to 1,2-PDO [23–32]. A key question that remains is the exact dehydration active site for the first step of glycerol hydrogenolysis (Scheme 1). Although glycerol dehydration is generally accepted to be catalyzed by acid or base supports, some disparate opinions still exist. For instance, Sun et al. [2] speculated that the carriers might not be able to catalyze glycerol dehydration to hydroxyacetone and behaved just as inert supports for dispersion of Cu after extensive literature investigation. They deduced that metallic Cu not only worked as an active hydrogenation center, but also involved glycerol dehydration. Especially, Raney Cu has been established to catalyze glycerol dehydration to hydroxyacetone [33]. Moreover, it is hard to produce hydroxyacetone selectively from glycerol dehydration over supports such as Al<sub>2</sub>O<sub>3</sub>, ZrO<sub>2</sub>, and TiO<sub>2</sub> [33,34]. For example, Cu/Al<sub>2</sub>O<sub>3</sub> exhibits glycerol conversion of 61% with 93.3% 1,2-PDO selectivity, while pure Al<sub>2</sub>O<sub>3</sub> gives a conversion of 7% without forming hydroxyacetone under identical reaction conditions [23]. Nevertheless, up to now, no direct experimental evidence has been obtained to

\* Corresponding author.

E-mail addresses: [zhushanhui@sxicc.ac.cn](mailto:zhushanhui@sxicc.ac.cn) (S. Zhu), [fanwb@sxicc.ac.cn](mailto:fanwb@sxicc.ac.cn) (W. Fan).

<sup>1</sup> These authors contributed equally to this work.



**Scheme 1.** Reaction route of glycerol hydrogenolysis into 1,2-PDO [2].

illustrate the exact roles of Cu and supports in glycerol dehydration. In this context, further research is necessary.

In the present work, excellent Cu/SBA-15 catalysts were prepared by a simple grinding method, and these catalysts were employed to identify the exact dehydration active site with some other catalysts as comparisons. It was found that the interfacial Cu—O—Si—O— structure played a decisive role in the dehydration process, which was confirmed by both experiments and density functional theory (DFT) calculation results. Copper species evolution in catalyst preparation processes was thoroughly investigated for the first time on Cu/SBA-15 by a grinding method.

## 2. Experimental

### 2.1. Catalyst preparation

The template-free SBA-15 was purchased from XF Nano Materials Tech. Nanjing Co. Ltd.  $x$ Cu/SBA-15(G) catalysts ( $x$  represents nominal Cu mass percentage) were obtained by grinding SBA-15 with a certain amount of  $\text{Cu}(\text{NO}_3)_2 \cdot 3\text{H}_2\text{O}$  at room temperature for 1 h in a planetary ball mill and subsequently calcined at 773 K for 5 h in an air flow. For comparison, 10%Cu/SBA-15(IM) was prepared by an incipient wetness impregnation method. The impregnated sample was dried at 373 K and calcined under the same conditions as those used for calcining  $x$ Cu/SBA-15(G).

Cu@SiO<sub>2</sub> was fabricated using the modified method reported by Zheng [35]. First, Cu powder (Alfa Aesar) was calcined at 573 K in air. After that, 0.3 g of the obtained powder and 2 g of cetyltrimethyl ammonium bromide (CTAB) were added to 300 mL deionized water. Then, 0.6 g tetraethyl orthosilicate (TEOS) and 5 mL ethanol were added to the mixture and it was stirred for 1 h. The solid products were then separated, washed, and dried, followed by calcination at 773 K for 5 h.

### 2.2. Characterization

The metal loadings in the catalysts were determined by inductively coupled plasma atomic emission spectroscopy (ICP-AES, Thermo iCAP6300).

N<sub>2</sub> physisorption measurements were performed at 77 K on a TriStar3020 II gas adsorption analyzer. Prior to the measurement, all the samples were treated at 593 K for 10 h under high vacuum to remove water and other physically adsorbed impurities.

The powder X-ray diffraction (XRD) patterns of  $x$ Cu/SBA-15(G) and 10%Cu/SBA-15(IM) were recorded on a Rigaku MiniFlex II X-ray diffractometer with CuK $\alpha$  radiation (30 kV and 15 mA) at a scanning speed of 4°min<sup>-1</sup>. The samples reduced at 593 K for 2 h under 10 vol% H<sub>2</sub>/Ar were protected with liquid paraffin for XRD measurement.

Temperature-programmed desorption of ammonia (NH<sub>3</sub>-TPD) was carried out in a Micromeritics Autochem II 2920 chemisorption analyzer equipped with a thermal conductivity detector (TCD). Before adsorption, an approximately 0.05-g sample was pre-reduced at 593 K for 2 h in 10 vol% H<sub>2</sub>/Ar (30 mL min<sup>-1</sup>) and then cooled to 393 K. Subsequently, the sample was purged with an NH<sub>3</sub>/He mixture (1:9 vol ratio) for 30 min. After that, the physisorbed NH<sub>3</sub> was removed by flushing the sample with pure helium (30 mL min<sup>-1</sup>) at 393 K for 2 h. Finally, the sample was heated from 393 to 773 K at a rate of 10 K min<sup>-1</sup>.

In situ diffuse reflectance Fourier transform infrared spectra (DRIFTS) were collected on a Nicolet iS10 FTIR spectrophotometer equipped with a SMART collector and an MCT detector cooled with liquid N<sub>2</sub>. Typically, a certain amount of KBr was first placed into the sample cell as background. Then about 5 mg of dried catalyst was added. The sample was heated to 693 K at a ramp rate of 2 K min<sup>-1</sup> in an air flow (15 mL min<sup>-1</sup>), and the DRIFTS spectra were simultaneously recorded.

The reduction behavior of catalysts was investigated by H<sub>2</sub> temperature-programmed reduction (H<sub>2</sub>-TPR) conducted in a Micromeritics AutoChem II 2920 chemisorption analyzer. Typically, a 50-mg sample was loaded into a U-type quartz tube and heated at 593 K for 30 min in flowing Ar. After the sample was cooled to room temperature, the pretreated catalyst was heated again to 973 K at a rate of 5 K min<sup>-1</sup> in a 10 vol% H<sub>2</sub>/Ar flow (30 mL min<sup>-1</sup>) and the consumed hydrogen concentration was monitored by a TCD at the same time.

N<sub>2</sub>O chemisorption was performed to determine copper specific surface area using the same apparatus as for H<sub>2</sub> TPR. First, 30 mg of catalyst was pre-reduced at 593 K for 2 h in a 10 vol% H<sub>2</sub>/Ar flow (15 mL min<sup>-1</sup>). Then it was immediately cooled to room temperature. Subsequently, the surface copper of the catalyst was oxidized to Cu<sub>2</sub>O in 5 vol% N<sub>2</sub>O/Ar (15 mL min<sup>-1</sup>) at 323 K for 20 min. Then the catalyst was reduced by a 10 vol% H<sub>2</sub>/Ar flow (15 mL min<sup>-1</sup>) with the temperature increasing from room temperature to 493 K, and the consumed hydrogen amount ( $H_{\text{Cu}_2\text{O}}$ ) was monitored. To determine the total hydrogen consumption, the sample was first oxidized to CuO at 573 K for 1 h in 1 vol% O<sub>2</sub>/Ar (15 mL/min). After that, it was heated from room temperature to 1173 K at a rate of 10 K/min in a 10 vol% H<sub>2</sub>/Ar flow (15 mL min<sup>-1</sup>), and the corresponding hydrogen consumption amount ( $H_T$ ) was detected. The specific surface area and dispersion of copper species can be calculated by the equations [36,37]

$$S_{\text{Cu}} = 2 \times H_{\text{Cu}_2\text{O}} \times N_{\text{Av}} / (H_T \times M_{\text{Cu}} \times 1.4 \times 10^{19}) \\ = 1353 \times H_{\text{Cu}_2\text{O}} / H_T (\text{m}^2/\text{g}_{\text{Cu}}),$$

$$D_{\text{Cu}} = (2 \times H_{\text{Cu}_2\text{O}} / H_T) \times 100\%,$$

where  $N_{\text{Av}}$  = Avogadro's constant,  $M_{\text{Cu}} = 63.46$  g/mol, and  $1.4 \times 10^{19}$  refers to the  $1.4 \times 10^{19}$  copper atoms per square meter, because the average surface area of a copper atom is 0.0711 nm<sup>2</sup>.

The Cu nanoparticle images were measured by transmission electron microscopy (TEM, JEM-2001F, JEOL, Japan) at 200 kV.

The X-ray photoelectron spectra (XPS) and X-ray induced Auger electron spectra (XAES) were measured on a Kratos AXIS ULTRA DLD spectrometer equipped with monochromated AlK $\alpha$  radiation and a multichannel detector. Notably, reduced samples were first pretreated in a 10% H<sub>2</sub>/Ar flow at different temperatures for 2 h in an auxiliary pretreatment chamber before XPS measurements. Then they were transferred to the XPS measurement chamber under high vacuum conditions without air exposure. The collected binding energy values were referenced to the C1s peak at 284.6 eV with an experimental error of  $\pm 0.1$  eV.

Fourier transform infrared spectra of pyridine adsorbing (Py-IR) samples were collected on a Bruker Tensor 27 FT-IR spectrometer. First, the sample was pressed into a self-supported wafer and placed in a vacuum cell. Prior to the measurement, the sample wafer was reduced by 10 vol% H<sub>2</sub>/Ar (50 mL min<sup>-1</sup>) at 593 K for

2 h, followed by evacuation at  $10^{-2}$  Pa for 2 h. Finally, pyridine vapor was introduced in the sample cell at 308 K for 1 h and the spectra were recorded after evacuation at 423 K for 15 min.

### 2.3. In situ Fourier transform infrared experiments of glycerol adsorption

In situ FT-IR experiments of glycerol adsorption were conducted on a Bruker Tensor 70 FT-IR spectrometer equipped with a LN-MCT Mid VP detector. A self-supported sample wafer was reduced with 10 vol%  $H_2/Ar$  flow ( $50\text{ mL min}^{-1}$ ) at 593 K for 2 h. The spectra were collected at selected temperatures in the course of cooling down and used as background. After cooling to room temperature,  $20\ \mu\text{L}$  5 wt% glycerol tetrahydrofuran solution was dripped onto the wafer homogeneously. The wafer was then heated, and the IR spectra were recorded under vacuum at 323, 373, 423, and 473 K. Tetrahydrofuran was used as a solvent because it can easily be pumped out of the vacuum system at room temperature for its low boiling point. The spectra of adsorbed species can be acquired by subtracting the background spectra. The weight of the sample wafer is about 10 mg for pure SBA-15, 10%Cu/SBA-15(IM), and 10%Cu/SBA-15(G). Cu+SBA-15 is a physical mixture of 50 wt% metallic Cu (Alfa-Aesa) with particle size 0.5–1.5  $\mu\text{m}$  diameter and 50 wt% SBA-15.

### 2.4. Density functional theory calculations

First principles DFT calculations were carried out with the Vienna ab initio simulation package (VASP) [38,39] with projector-augmented wave (PAW) [40,41] pseudo-potentials. The generalized gradient approximation (GGA)-type functional, parameterized by Perdew, Burke, and Ernzerhof (PBE), was implemented to describe electron exchange and correlation energy [42]. The plane-wave cutoff energy for the wave function was set to 400 eV. All structures were considered relaxed until the total energy was converged to  $10^{-5}$  eV and all atomic forces were smaller than  $0.05\text{ eV \AA}^{-1}$ . Spin-polarized calculations were performed. We adopted a four-layer  $\text{SiO}_2$  (1 1 0) slab with a  $\text{Cu}_4$  adsorbing structure ( $\text{Cu}_4/\text{SiO}_2$ ) to investigate the Cu–O–Si–O– interface interaction. More details concerning DFT methods and the calculated model are described in the [Supplementary Material](#).

### 2.5. Catalytic test

Glycerol hydrogenolysis to 1,2-PDO was carried out in a Teflon-lined stainless steel autoclave (NS-10-316 L, Anhui Kemi Machinery Technology Co., Ltd.) equipped with an electromagnetic stirrer and a temperature controller. The specific reaction conditions were as follows: a certain amount of catalyst, 6.67 g n-butanol solution of glycerol (12 wt%), 483 K, 4.0 MPa hydrogen pressure, and 500 rpm stirring speed. All the catalysts were pre-reduced in a flow of 10 vol%  $H_2/Ar$  ( $50\text{ mL min}^{-1}$ ) at 593 K for 2 h before reaction. After designed reaction time, the reactor was cooled with an ice water bath. Finally, the used catalyst was separated from the liquid phase by centrifugation.

The collected liquid samples were analyzed on a Shimadzu GC-2010 Plus gas chromatograph equipped with a flame ionization detector (FID), an HP-PONA capillary column, and an autosampler. The gas phase was analyzed on an Agilent 7890A gas chromatograph equipped with two FIDs, a TCD, two capillary columns (DB-1 and GS-OxyPlot), and a  $\text{Al}_2\text{O}_3/\text{KCl}$  column. The gaseous products contain little  $\text{CO}_2$ . The contents of products and unreacted glycerol were determined using an external standard method. The conversion of glycerol, selectivity to identified products, and turnover frequency (TOF) were calculated as follows:

$$\text{Glycerol conversion} = \left(1 - \frac{\text{moles of unreacted glycerol}}{\text{moles of glycerol in the feed}}\right) \times 100\%$$

$$1,2\text{-PDO selectivity} = \frac{\text{moles of 1,2-PDO}}{\text{moles of all liquid products}} \times 100\%$$

$$\text{TOF (h}^{-1}\text{)} = \frac{\text{conversion} \times \text{moles of glycerol in the feed (mol)}}{\text{total Cu amount (mol)} \times \text{Cu dispersion} \times \text{reaction time (h)}}$$

## 3. Results and discussion

### 3.1. Formation of Cu–O–Si–O– species and highly dispersed Cu

XPS analysis was used to determine the chemical states of copper. The XPS spectra of calcined and reduced 10%Cu/SBA-15(G) and 10%Cu/SBA-15(IM) are shown in [Fig. 1A](#). For calcined 10%Cu/SBA-15(G), two Cu  $2p_{3/2}$  peaks (933.1 eV and 935.4 eV) can be distinguished, corresponding to CuO and Cu–O–Si–O– species, respectively [32,43–45]. As a comparison, the 935.4 eV peak of calcined 10%Cu/SBA-15(IM) is much smaller and enveloped by the CuO peak at 933.1 eV, meaning fewer Cu–O–Si–O– species in calcined 10%Cu/SBA-15(IM). These results are supported by the green color of 10%Cu/SBA-15(G) and the gray color of 10%Cu/SBA-15(IM) shown in [Fig. S1 in the Supplementary Material](#), because the colors of Cu–O–Si–O– and bulk CuO are green and black, respectively [31].

From XPS spectra of reduced samples, it can be found that no satellite peak appears at 940–947 eV, suggesting that almost all of the  $\text{Cu}^{2+}$  species were reduced [46]. Additionally, the  $\text{Cu}2p_{2/3}$  binding energy of reduced 10%Cu/SBA-15(G) is higher than that of the sample prepared by impregnation. The shift of the reduced 10%Cu/SBA-15(G) to higher binding energy indicates that a strong interaction exists between Cu and  $\text{SiO}_2$  resulting from formation of Cu–O–Si bonds [47]. In contrast, only a few Cu–O–Si bonds were formed in 10%Cu/SBA-15(IM), as indicated by the asymmetry of the  $\text{Cu}2p_{2/3}$  peak. The electron shift in Cu–O–Si bonds should result in the formation of  $\text{Cu}^{\delta+}$  sites. To confirm the existence of Cu–O–Si–O– species and determine the surface content of Cu species with different valence states, Cu LMM XAES spectra were recorded for reduced catalysts ([Fig. 1B](#)). All samples presented two peaks at kinetic energies of about 918.1 and 914.2 eV in the Cu LMM XAES spectra, which could be ascribed to  $\text{Cu}^0$  and  $\text{Cu}^{\delta+}$  sites (Cu–O–Si–O– species), respectively [3,37].  $(\text{Cu–O–Si–O–})/\text{Cu}^0$  was calculated by the area ratio of peaks centered at 914.2 and 918.1 eV. As clearly illustrated in [Fig. 1B](#), the  $(\text{Cu–O–Si–O–})/\text{Cu}^0$  ratio of 10%Cu/SBA-15(G) (1.098) was much higher than that of 10%Cu/SBA-15(IM) (0.706), coincident with XPS results.

The TEM images of reduced 10%Cu/SBA-15(IM) and xCu/SBA-15(G) are shown in [Fig. S2](#). Initially, no obvious Cu nanoparticles could be found in the general microstructure of reduced ground samples ([Figs. S2A, S2C, and S2E](#)); the Cu nanoparticles are probably located inside the mesopores of SBA-15 [48]. After being exposed to electron beam irradiation at high resolution for about 5 min, the ordered mesopores of SBA-15 were damaged and Cu nanoparticles showed up ([Figs. S2B, S2D, and S2F](#)). The Cu nanoparticles in xCu/SBA-15(G) are highly dispersed and the particle sizes are small. However, the large Cu particles could easily be identified for 10%Cu/SBA-15(IM) ([Fig. S2H](#)), suggesting that small Cu nanoparticles could be obtained more easily by grinding than impregnation.

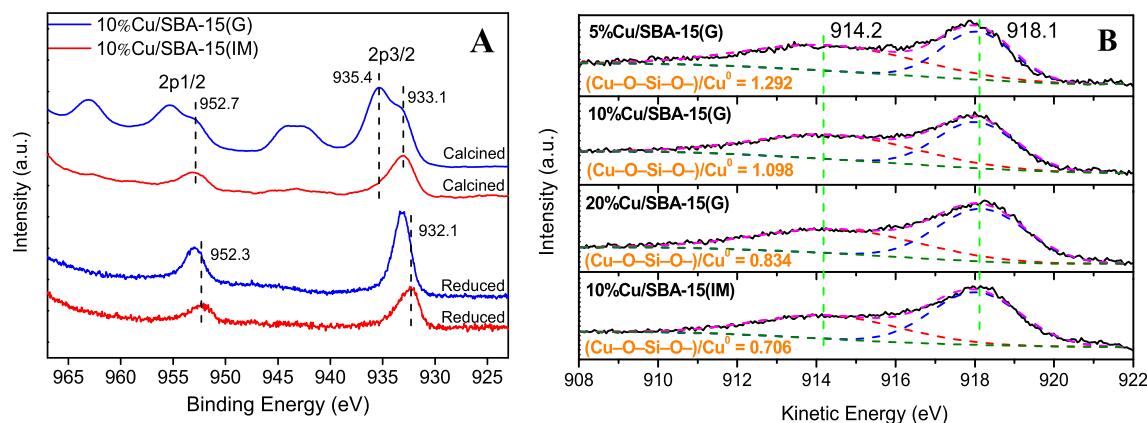


**Fig. 1.** (A) XPS spectra of calcined and reduced samples with 10 wt% Cu loading synthesized by grinding and impregnation. (B) Deconvolution of Cu XAES spectra of reduced catalysts.

To illustrate the effects of the two preparation methods, XRD patterns of 10%Cu/SBA-15(G) and 10%Cu/SBA-15(IM) at different stages were recorded to analyze the structural evolution during synthesis. As displayed in Fig. 2A, the diffraction peaks at  $12.6^\circ$ ,  $25.6^\circ$ , and  $33.4^\circ$  are ascribed to copper hydroxynitrate ( $\text{Cu}_2(\text{OH})_3\text{NO}_3$ ) of dried 10%Cu/SBA-15(IM) [22]. The sharp diffraction peaks indicate aggregation of copper salt in the drying process. After calcination at 773 K for 5 h, the  $\text{Cu}_2(\text{OH})_3\text{NO}_3$  diffraction peaks were totally replaced by CuO peaks at  $35.4^\circ$ ,  $38.6^\circ$ , and  $48.7^\circ$ . After reduction at 593 K, these peaks for CuO disappeared and peaks of Cu showed up. However, no obvious diffraction peaks related to copper species can be observed in XRD spectra of the dried, calcined, and reduced 10%Cu/SBA-15(G) (Fig. 2B). These results suggest that good dispersion of  $\text{Cu}_2(\text{OH})_3\text{NO}_3$ , CuO, and Cu can be obtained at different stages for the ground catalyst. Xie et al. [49] pointed that nitrates can be highly dispersed on the surfaces of supports ( $\gamma\text{-Al}_2\text{O}_3$ ,  $\text{TiO}_2$ , zeolites, etc.) at temperatures much lower than their melting temperatures. During grinding, strong friction leads to an increase in the surface temperature of  $\text{Cu}_2(\text{OH})_3\text{NO}_3$  particles, which facilitates the dispersion of the Cu precursor. However, with the impregnation method, the copper precursor tends to aggregate at the drying stage, as confirmed by XRD. By comparing the XRD patterns of 10%Cu/SBA-15(G) and 10%Cu/SBA-15(IM), it can be inferred that better dispersion of  $\text{Cu}_2(\text{OH})_3\text{NO}_3$  on SBA-15 leads to smaller CuO and Cu particles after calcination and reduction, respectively, and the mechanical mixing step is a decisive factor for well-dispersed Cu on xCu/SBA-15(G).

IR spectroscopy is a superior tool to distinguish  $\text{Cu}(\text{OH})_2$ ,  $\text{Cu}_2(\text{OH})_3\text{NO}_3$ , and Cu–O–Si–O– species [43]. To confirm the decisive role of grinding, in situ DRIFTS was employed to study the evolution of copper species in calcination processes. Fig. 3 shows the DRIFTS spectra of dried 10%Cu/SBA-15(G) and 10%Cu/SBA-15(IM) collected in situ at different calcination temperatures. At 313 K, two absorption bands were observed at approximately  $1430$  and  $1349$   $\text{cm}^{-1}$ , which are related to  $\text{NO}_3$  groups [50,51] and imply the presence of  $\text{Cu}_2(\text{OH})_3\text{NO}_3$ .

With the increase in calcination temperature,  $\text{Cu}_2(\text{OH})_3\text{NO}_3$  decomposed and its characteristic peaks disappeared. The  $\delta_{\text{OH}}$  band could be found at  $670$   $\text{cm}^{-1}$  for both calcined catalysts, and is generally assigned to OH deformation vibration of copper phyllosilicate in previous Refs. [3,43,50,52]. In our work, the surface Cu–O–Si–O– species have formation processes and chemical structures similar to those of copper phyllosilicate, and thus we deduce that the  $\delta_{\text{OH}}$  may be related to surface hydroxyl groups of Cu–O–Si–O– species. Notably, the peak around  $800$   $\text{cm}^{-1}$  in the spectra of 10%Cu/SBA-15(G) became weaker and the  $1120$   $\text{cm}^{-1}$  band became stronger (Fig. 3A) during calcination. Nevertheless,

these two peaks did not show much change over 10%Cu/SBA-15(IM) (Fig. 3B). The absorption bands around  $800$  and  $1120$   $\text{cm}^{-1}$  are assigned to different vibration modes of Si–O bonds of silica [3,50,53]. Because the existence of a Cu–O–Si–O– structure has been confirmed by the color of the catalyst (Fig. S1), the XPS peak at  $935.4$  eV (Fig. 1A), and XAES peaks at  $914.2$  eV (Fig. 1B), the increasing intensity of Si–O vibration ( $1120$   $\text{cm}^{-1}$ ) was probably also relevant to the formation of large numbers of Si–O bonds related to Cu–O–Si–O– structure in 10%Cu/SBA-15(G). As reported by Gong and his co-workers [43],  $\text{Cu}^{2+}$  can react with the silanol groups of a silica surface to produce  $\equiv\text{SiOCu}^{\text{II}}$  monomers and form Cu–O–Si–O– via consecutive polymerization. After grinding, the well-dispersed copper precursor can react with silanol groups at the interface of  $\text{Cu}_2(\text{OH})_3\text{NO}_3$  and SBA-15. It is reasonable to deduce that better-dispersed  $\text{Cu}_2(\text{OH})_3\text{NO}_3$  obtained by grinding can interact more easily with silanol groups on the SBA-15 surface, resulting in more Cu–O–Si–O– species formation. The Cu–O–Si–O– structure between the interface of copper species and SBA-15 can stabilize the CuO and Cu nanoparticles in the calcination and reduction steps. For 10%Cu/SBA-15(IM), bulk  $\text{Cu}_2(\text{OH})_3\text{NO}_3$  results in a small interface between  $\text{Cu}_2(\text{OH})_3\text{NO}_3$  and SBA-15 and much fewer Cu–O–Si–O– species can be formed, leading to formation of bulk CuO and Cu.

From these discussions, it can be found that the formation of fine dispersed copper precursor by grinding plays a key role in the synthesis of highly dispersed Cu/SBA-15 catalyst. These findings suggest pursuing high dispersion of metallic precursors to construct well supported catalysts.

### 3.2. Structure–performance relationship

The reduced catalysts were evaluated at 483 K and 4.0 MPa hydrogen pressure with n-butanol as solvent for different reaction times. As displayed in Fig. 4A, the conversion of glycerol gradually increased with increasing reaction time. For 10%Cu/SBA-15(G), glycerol conversion was 59.1% at 1.5 h and increased to 88.9% in another 4.5 h. Comparatively, the impregnated catalyst exhibited much lower glycerol conversion for all the tests, despite that both catalysts showed excellent selectivity to 1,2-PDO > 97% due to the higher intrinsic ability of Cu-based catalysts to selectively cleave C–O bonds over C–C bonds [2].

Fig. 4B illustrates the effects of Cu loading on the catalytic performance of glycerol hydrogenolysis over Cu/SBA-15(G). Glycerol conversion improved from 40.1% to 70.6% with Cu content increasing from 5% to 20% at reaction time of 1.5 h, while the selectivity to 1,2-PDO declined only slightly. Reactions performed under other conditions (different temperatures and atmospheres) were also

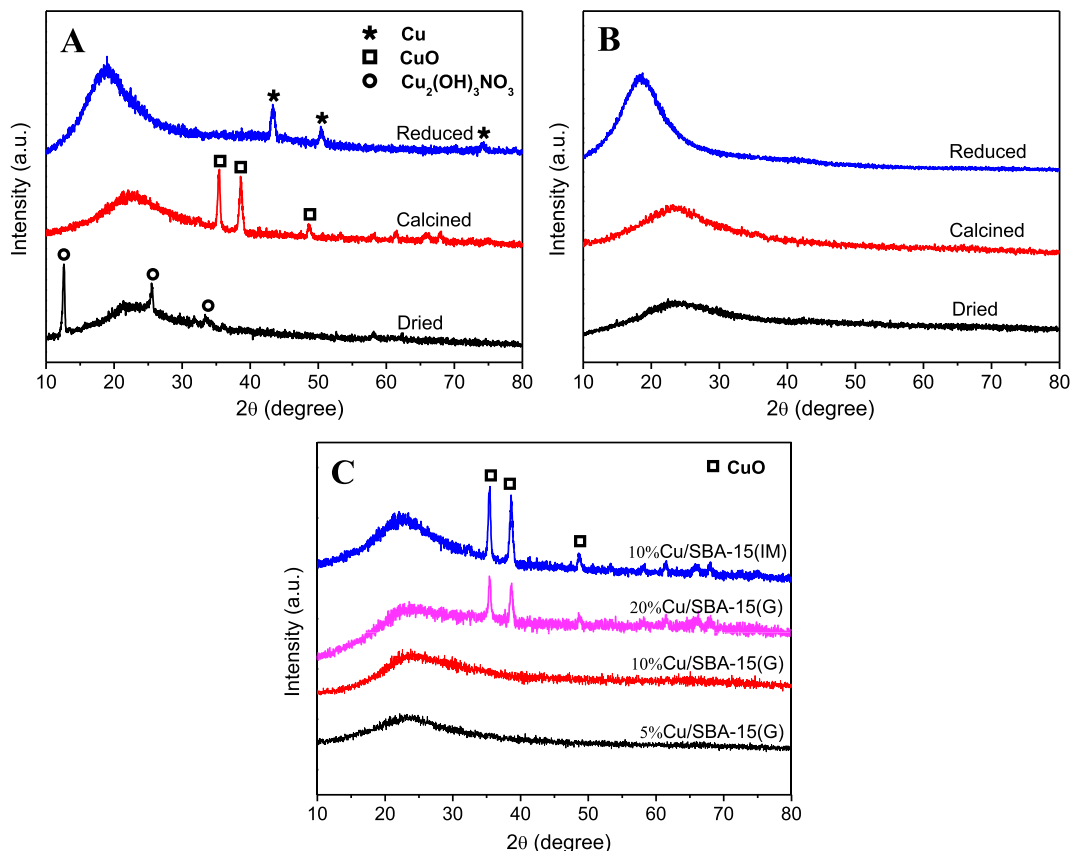


**Fig. 2.** XRD patterns of dried, calcined, and reduced (A) 10%Cu/SBA-15(IM) and (B) 10%Cu/SBA-15(G). (C) Comparison of XRD results for calcined 10%Cu/SBA-15(IM) and xCu/SBA-15(G).

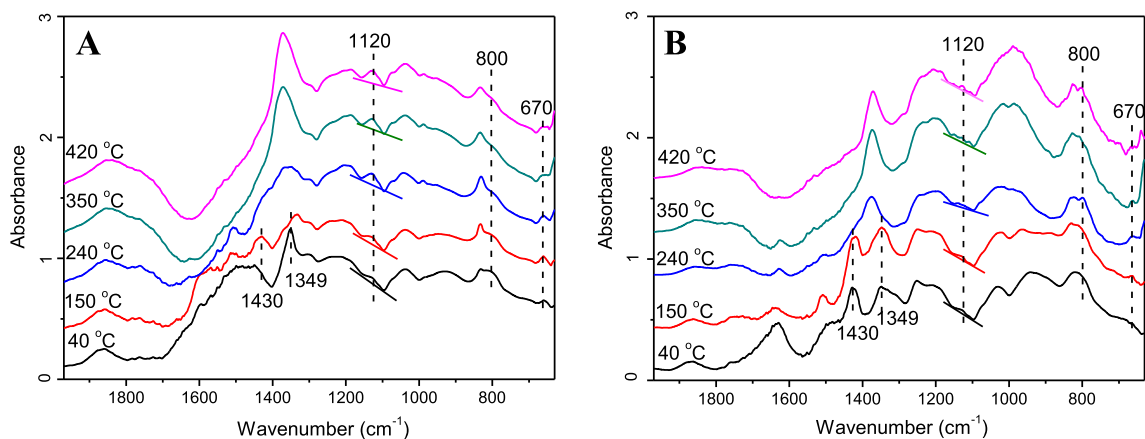


**Fig. 3.** In situ DRIFTS spectra of 10%Cu/SBA-15(G) (A) and 10%Cu/SBA-15(IM) (B).

investigated for 10%Cu/SBA-15(IM) and 10%Cu/SBA-15(G) (Table 1). An increase of reaction temperature greatly enhanced the conversion of glycerol.

The structural and surface properties of employed catalysts were analyzed to disclose their different catalytic performance. Fig. S3 shows the N<sub>2</sub> adsorption–desorption isotherms and pore size distribution curves of calcined catalysts, SBA-15, and ground SBA-15 (SBA-15(G)). The surface area and pore volume are listed in Table 2. After ball-milling, a decrease in volume and surface area was observed for SBA-15, indicating that the milling step damaged

its structure. For all the calcined catalysts, the surface area and pore volume are proportionally decreased with increased copper content.

The exposed copper surface area, dispersion, and Cu crystallite size were measured by the N<sub>2</sub>O dissociative chemisorption method. As shown in Table 2, 10%Cu/SBA-15(IM) shows the lowest dispersion (8.8%), while the dispersion of 10%Cu/SBA-15(G) is about six times higher. These results clearly suggest that the grinding method facilitates the formation of small, highly dispersed Cu nanoparticles. Among the ground samples, 5%Cu/SBA-15(G) shows

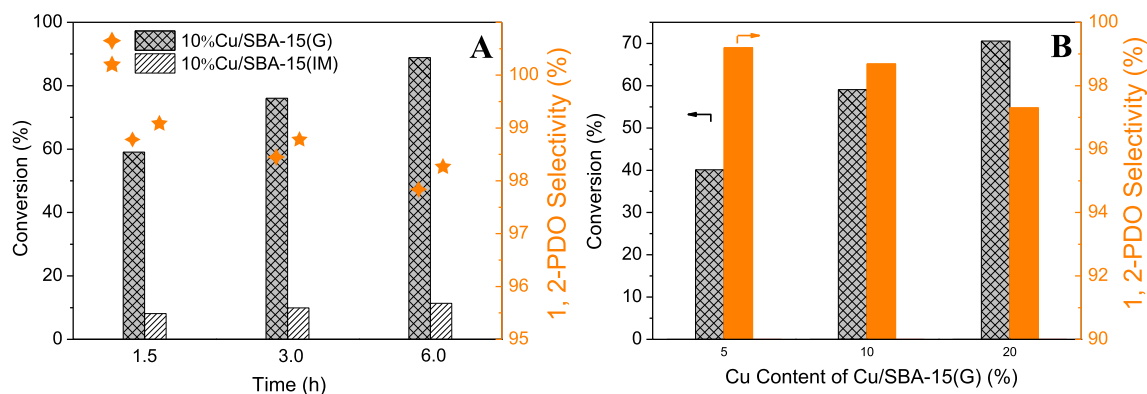


**Fig. 4.** Glycerol conversion and 1,2-PDO selectivity of 10%Cu/SBA-15(G) and 10%Cu/SBA-15(IM) at different reaction times (A), and of xCu/SBA-15(G) at a TOS of 1.5 h (B). Reaction conditions: 4.0 MPa, 483 K, weight ratio of catalyst/glycerol = 1:10.

**Table 1**

Catalytic results for hydrogenolysis of glycerol on 10%Cu/SBA-15(IM) and 10%Cu/SBA-15(G) under different conditions.<sup>a</sup>

Sample	T (K)	Atmosphere	Conversion (%)	Selectivity (%)			Carbon balance (%)
				1,2-PDO	Hydroxyacetone <sup>b</sup>	Others	
10%Cu/SBA-15(IM)	443	H <sub>2</sub> 4 MPa	1.5	99.3	—	~0.7 <sup>c</sup>	95.4
	463	H <sub>2</sub> 4 MPa	3.3	98.9	—	~1.1 <sup>c</sup>	95.9
	483	H <sub>2</sub> 4 MPa	8.1	99.2	—	~0.8 <sup>c</sup>	96.1
	503	H <sub>2</sub> 4 MPa	13.6	97.5	—	~2.5 <sup>c</sup>	95.1
	483	N <sub>2</sub> 4 MPa	1.6	0	50.5	49.5 <sup>d</sup>	—
10%Cu/SBA-15(G)	443	H <sub>2</sub> 4 MPa	8.7	99.5	—	~0.5 <sup>c</sup>	94.1
	463	H <sub>2</sub> 4 MPa	24.9	99.2	—	~0.8 <sup>c</sup>	95.2
	483	H <sub>2</sub> 4 MPa	59.1	98.7	—	~1.3 <sup>c</sup>	93.8
	503	H <sub>2</sub> 4 MPa	90.3	97.3	—	~2.7 <sup>c</sup>	94.6
	483	N <sub>2</sub> 4 MPa	7.5	0	56.9	43.1 <sup>d</sup>	—

<sup>a</sup> Other reaction conditions: 1.5 h, weight ratio of catalyst/glycerol = 1:10.

<sup>b</sup> Hydroxyacetone can be detected by GC, but its quantity is too small to quantify.

<sup>c</sup> Others include ethylene glycerol and propanols.

<sup>d</sup> Compounds that cannot be defined.

**Table 2**

The physiochemical properties of different samples.

Sample	Cu content (wt.%) <sup>a</sup>	S <sub>BET</sub> (m <sup>2</sup> g <sup>-1</sup> )	V <sub>p</sub> (cm <sup>3</sup> g <sup>-1</sup> )	Calculated by N <sub>2</sub> O chemisorption results			Acid site amount <sup>e</sup> (μmol/g)
				D (%) <sup>b</sup>	d <sub>Cu</sub> (nm) <sup>c</sup>	S <sub>Cu</sub> (m <sup>2</sup> <sub>Cu</sub> g <sub>cat</sub> <sup>-1</sup> ) <sup>d</sup>	
SBA-15	—	608	0.99	—	—	—	0.004
10%Cu/SBA-15(IM)	9.6	490	0.85	8.8	11.3	5.9	0.105
SBA-15(G)	—	471	0.65	—	—	—	0.004
5%Cu/SBA-15(G)	4.9	406	0.56	70.0	1.4	23.2	0.560
10%Cu/SBA-15(G)	9.7	366	0.51	54.9	1.8	37.1	0.851
20%Cu/SBA-15(G)	19.3	267	0.43	38.6	2.6	50.4	1.047
Cu powder <sup>f</sup>	—	—	—	8.3	—	5.6	—
Cu@SiO <sub>2</sub>	—	—	—	7.1	—	4.8	0.072

<sup>a</sup> Determined by ICP.

<sup>b</sup> Dispersion degree of metallic copper.

<sup>c</sup> Average size of Cu particles.

<sup>d</sup> Cu exposed surface area calculated from N<sub>2</sub>O chemisorption (Fig. S4).

<sup>e</sup> Determined by NH<sub>3</sub> TPD.

<sup>f</sup> Metallic Cu powder purchased from Alfa-Aesar.

the highest Cu<sup>0</sup> dispersion (70.0%). Although the dispersion degree decreases with the increase in the copper amount, it still remains at a high value of 38.6% when the sample supports 20% Cu.

The H<sub>2</sub>-TPR profiles of both 10%Cu/SBA-15(IM) and 20%Cu/SBA-15(G) show two reduction peaks (Fig. 5). The low-temperature peak at 460–470 K is related to the reduction of well-dispersed CuO nanoparticles, while the high-temperature one (550 K) can be ascribed to bulk CuO [22,23]. It is noteworthy that the high-temperature reduction peak area is much larger than the low-temperature peak area in the profile of 10%Cu/SBA-15(IM), whereas the H<sub>2</sub>-TPR profile of 20%Cu/SBA-15(G) is dominated by

the low-temperature peak, and only one peak at 460–470 K can be found when Cu content is decreased to 10% or 5%. This gives another piece of evidence for the conclusion that most copper species in 10%Cu/SBA-15(IM) are bulk CuO, while the samples prepared by the grinding method contain mainly highly dispersed CuO nanoparticles. The slight shift of the reduction peak at about 460 K to higher temperature with increasing Cu loading in the ground catalysts indicates an increase of CuO nanoparticle size. The above results confirm that much higher Cu<sup>0</sup> dispersion could be achieved by grinding than by the conventional impregnation method, in line with XRD, N<sub>2</sub>O dissociative chemisorption, and

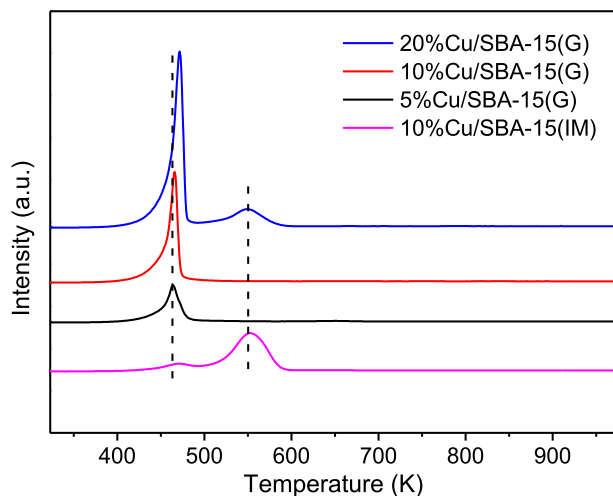


Fig. 5. H<sub>2</sub> TPR profiles of xCu/SBA-15(G) and 10%Cu/SBA-15(IM).

TEM characterization results. It is generally accepted that metallic Cu is the active site for hydroxyacetone hydrogenation [2], which is the second step of glycerol hydrogenolysis (Scheme 1). Thus, more 1,2-PDO could be obtained over a larger exposed Cu surface area if more hydroxyacetone could be provided from the first dehydration step.

It was mentioned in [29] that metallic Cu species might also catalyze glycerol dehydration to hydroxyacetone. To identify the exact role of Cu<sup>0</sup>, glycerol hydrogenolysis reactions were performed on SBA-15, Cu powder, and a mixture of Cu powder and SBA-15 (Cu+SBA-15). The catalytic results listed in Table S1 show that Cu powder exhibited a much lower reaction rate than 10% Cu/SBA-15(IM) under the same conditions, although their exposed Cu<sup>0</sup> surfaces were very close. Because 10%Cu/SBA-15(IM) possesses a certain amount of Cu–O–Si–O– structure, absence of Cu–O–Si–O– structure seems very likely to be the reason for poor catalytic activity of Cu powder and Cu+SBA-15.

Py-IR spectra of reduced samples in Fig. S5 illustrate that 10% Cu/SBA-15(IM) and xCu/SBA-15(G) possess only Lewis acid sites (LAS), while the acid site amount is negligible for SBA-15 and Cu +SBA-15. According to XPS and XAES results of reduced catalysts (Fig. 1), the Cu–O–Si–O– structure should be the only source of Lewis acid [42,51,52,54]. The acid site amounts determined by NH<sub>3</sub>-TPD of the reduced 10%Cu/SBA-15(IM), 5%Cu/SBA-15(G), 10% Cu/SBA-15(G), and 20%Cu/SBA-15(G) are 0.105, 0.560, 0.851, and 1.047 mmol/g, respectively (Table 2). The much lower Lewis acid amount of 10%Cu/SBA-15(IM) than of xCu/SBA-15(G) further confirms that many more Cu–O–Si–O– structures were formed in xCu/SBA-15(G).

TOF can be employed to reflect the intrinsic activity of a catalyst, which has been estimated in terms of the surface-active Cu sites using initial glycerol conversion (<15%) (Table 3). Of all the examined catalysts, 5%Cu/SBA-15(G) achieved optimal performance, 57.2 h<sup>-1</sup>, which is superior to that of most reported Cu-based catalysts [2,5,24–29]. More interestingly, a strong linear relationship between TOF and LAS/Cu<sup>0</sup> was found, as displayed in Fig. 6A. LAS/Cu<sup>0</sup> indicates the LAS amount per Cu<sup>0</sup> site. It can be demonstrated that Lewis acid sites derived from Cu–O–Si–O– structures benefit the catalytic activity of Cu/SBA-15. Increasing numbers of Cu–O–Si–O– structures facilitate the continuous increase of TOF. The linear relationship between TOF and LAS/Cu<sup>0</sup> implies that Cu–O–Si–O– structures are crucial for achieving excellent hydrogenolysis performance. To make the conclusion more credible, Cu LMM X-ray excited XAES spectra were analyzed to reconfirm the (Lewis acid sites originated from Cu–O–Si–O–)/

Table 3

TOF and LAS/Cu<sup>0</sup> of xCu/SBA-15(G).

Samples	Conversion (%) <sup>a</sup>	LAS/Cu <sup>0b</sup>	TOF (h <sup>-1</sup> ) <sup>c</sup>
5%Cu/SBA-15(G)	7.3	1.017	57.2
10%Cu/SBA-15(G)	10.5	0.985	52.8
20%Cu/SBA-15(G)	13.5	0.862	48.3
10%Cu/SBA-15(IM)	1.4	0.758	44.2

<sup>a</sup> Reaction conditions: 4.0 MPa, 483 K, 1.0 h, weight ratio of catalysts/glycerol = 0.025.

<sup>b</sup> The Cu<sup>0</sup> site was determined from the metallic Cu dispersion ( $D_{Cu}$ ) measured by N<sub>2</sub>O chemisorption using the equation Cu<sup>0</sup> site amount per gram of catalyst =  $\frac{1 \text{ g} \times \text{Cu mass percentage}}{M_{Cu}} \times D_{Cu}$  (mol/g), where  $M_{Cu}$  = 63.46 g/mol.

<sup>c</sup> TOF was calculated on the basis of metallic Cu dispersion at conversions lower than 15% in this table.

Cu<sup>0</sup> ratio and the linear relationship between TOF and (Cu–O–Si–O–)/Cu<sup>0</sup>. As shown in Fig. 1B, the (Cu–O–Si–O–)/Cu<sup>0</sup> ratios of the reduced 10%Cu/SBA-15(IM), 5%Cu/SBA-15(G), 10%Cu/SBA-15(G), and 20%Cu/SBA-15(G) were 0.706, 0.834, 1.098, and 1.292, respectively. From Fig. 6B, TOF increased linearly with the rising ratio of (Cu–O–Si–O–)/Cu<sup>0</sup>, indicating the crucial role of the Cu–O–Si–O– structure in glycerol hydrogenolysis.

It can be speculated that Lewis acid sites originated from Cu–O–Si–O– might be the active center for catalyzing glycerol dehydration to hydroxyacetone, and the generated intermediate would adsorb onto adjacent Cu<sup>0</sup> sites for subsequent hydrogenation. Then, the high TOF of 5%Cu/SBA-15(G) can be ascribed to large numbers of Cu–O–Si–O– structures around Cu<sup>0</sup> sites.

Former research [55–57] have found that the rate-determining step of glycerol hydrogenolysis is the cleavage of C–OH bonds in the dehydration step rather than the hydrogenation of the dehydration product (hydroxyacetone). To prove this point, first, hydrogenation of hydroxyacetone was investigated on different catalysts. As shown in Table 4, the conversion of hydroxyacetone for 10 min at 443 K was 70.3% and 100% on 10%Cu/SBA-15(IM) and 10%Cu/SBA-15(G), respectively. However, glycerol conversion was only 1.5% and 8.7% on 10%Cu/SBA-15(IM) and 10%Cu/SBA-15(G), respectively, even for a much longer time (1 h) at the same temperature (Table 1). Thus, the hydrogenation of hydroxyacetone was proved not to be the rate-determining step, and could be effectively catalyzed by metallic Cu. These results evidenced that the promotion effect of Cu–O–Si–O– structures was mainly present in the dehydration step in this study.

For ground Cu/SBA-15 catalysts, the (Cu–O–Si–O– induced Lewis acid sites)/Cu<sup>0</sup> ratio increased with the decrease of Cu loading (Table 3). Thus, two other ground catalysts with 1% and 2% Cu loading were synthesized to get a high (Cu–O–Si–O–)/Cu<sup>0</sup> ratio for finding out the boundary of the linear relationship between TOF and (Cu–O–Si–O–)/Cu<sup>0</sup>. However, a good linear relationship between TOF and LAS/Cu<sup>0</sup> can still be observed over 1% and 2% Cu/SBA-15(G) in Fig. S6. Although the accurate boundary cannot be deduced with this result, the promotion effect of Cu–O–Si–O– structures was further confirmed.

### 3.3. In situ Fourier transform infrared experiments on glycerol adsorption

To probe the intrinsic active sites of glycerol dehydration, in situ FT-IR spectra were recorded at specified temperatures after adsorption of glycerol onto pure SBA-15, Cu+SBA-15, and reduced Cu/SBA-15 catalysts (Fig. 7). As shown in Fig. 7A, the initial glycerol loadings were almost the same on four samples because nearly identical infrared bands of adsorbed glycerol were observed at 1462 cm<sup>-1</sup> ( $\delta_{CH_2}$  of glycerol) and 1413 cm<sup>-1</sup> ( $\delta_{OH}$  of glycerol) [58]. The negative peak at about 1626 cm<sup>-1</sup> was ascribed to adsorbed H<sub>2</sub>O [34]. When the temperature was increased to

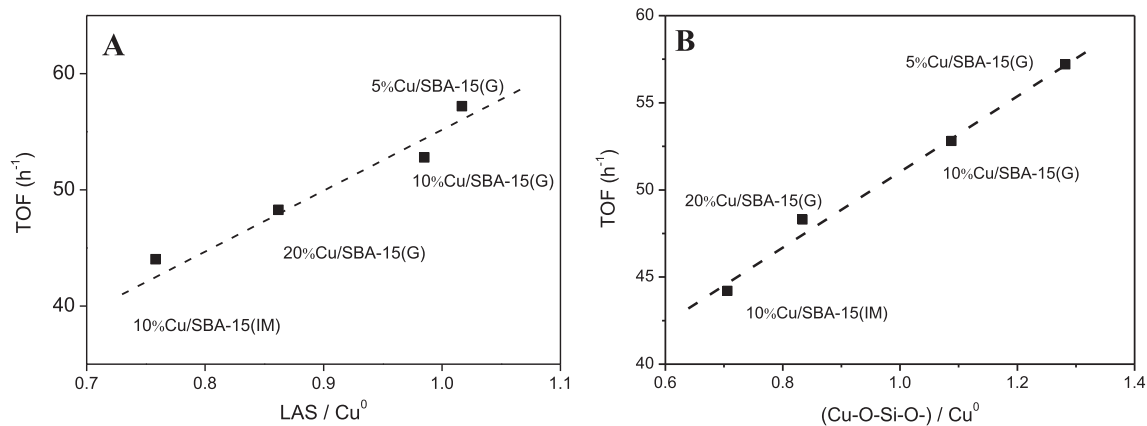


**Fig. 6.** (A) Relationship between LAS/Cu<sup>0</sup> and TOF of Cu<sup>0</sup>. (B) Relationship between (Cu–O–Si–O)/Cu<sup>0</sup> and TOF of Cu<sup>0</sup>.

**Table 4**  
Catalytic performance of hydroxyacetone hydrogenation on different catalysts.

Sample	Conversion (%)	1,2-PDO Selectivity (%)
Cu powder	55.9	>99
10%Cu/SBA-15(IM)	78.1	>99
10%Cu/SBA-15(G)	100	>99

Note: Reaction conditions: 4.0 MPa H<sub>2</sub>; 443 K; 10 min; molar quantity of hydroxyacetone equal to that of glycerol in hydrogenolysis reactions.

373 K (Fig. 7B), the amount of adsorbed glycerol decreased due to desorption of physically adsorbed glycerol at higher temperature. Nevertheless, more glycerol adsorbed onto the 10%Cu/SBA-15(G)

than onto the other samples, which suggested stronger interaction between glycerol and 10%Cu/SBA-15(G). With increasing temperature, the  $\delta_{\text{OH}}$  bands of glycerol at about 1413 cm<sup>-1</sup> [58] disappeared in the spectra of 10%Cu/SBA-15(G) and 10%Cu/SBA-15(IM) taken at 423 K and 473 K (Fig. 7C and D) because of dehydration of glycerol. For SBA-15 and Cu+SBA-15, the  $\delta_{\text{OH}}$  bands of glycerol became weaker and underwent a red shift at high temperature.

It should be noted that a broad peak in the 1600–1500 cm<sup>-1</sup> region started to appear at 373 K and became much more obvious at higher temperatures for 10%Cu/SBA-15(G) and 10%Cu/SBA-15(IM) (Fig. 7). In contrast, this band was much smaller in the spectrum of Cu+SBA-15 and could not be found for pure SBA-15. The band in the 1600–1500 cm<sup>-1</sup> region was attributed to carboxylate

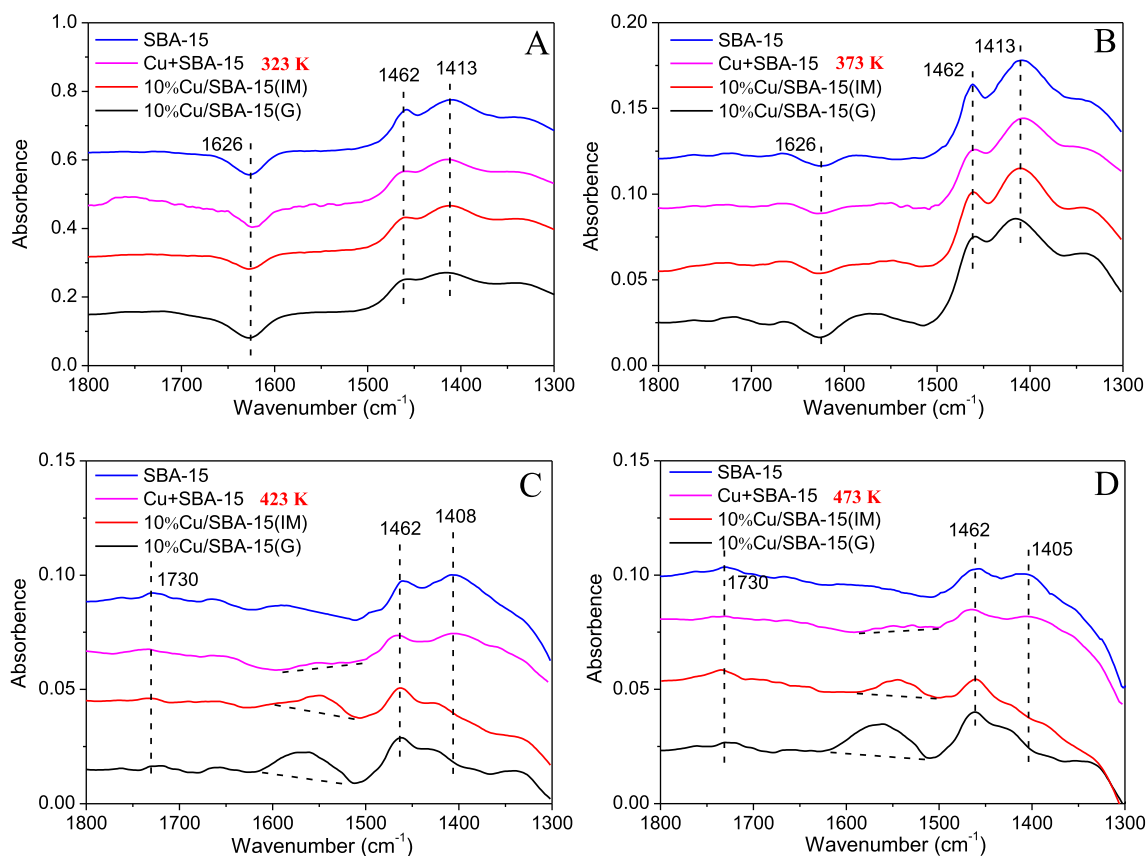


**Fig. 7.** In situ FT-IR spectra recorded at different temperatures after adsorbing glycerol.

species; it comes from the redox reaction between the copper species and hydroxyacetone under hydrogen-deficient conditions [59–61]. The much stronger band at 1600–1500  $\text{cm}^{-1}$  implies that more hydroxyacetone was produced on 10%Cu/SBA-15(G). Besides, the formation of hydroxyacetone can also be verified by the peak of  $\nu_{\text{C=O}}$  at 1730  $\text{cm}^{-1}$  [59,60]. The assignment of the 1600–1500  $\text{cm}^{-1}$  band was further demonstrated by hydroxyacetone adsorption experiments. Fig. S7 shows that this band appeared immediately after introduction of hydroxyacetone at 423 K. Thus, low conversion of glycerol under  $\text{N}_2$  can be explained (Table 1). Under hydrogen-deficient conditions, the generated carboxylate species covered the Cu surface and inhibited the dehydration reaction.

The above results indicate that Cu and SBA-15 are not effective catalysts for glycerol dehydration. Comparatively, 10%Cu/SBA-15(G) and 10%Cu/SBA-15(IM) are much more active, as confirmed by the high disappearance rate of glycerol hydroxyls with increasing temperature (Fig. 7). Thus, it can be concluded that metallic Cu and SBA-15 are not the primary dehydration active site, whereas Lewis acid sites derived from Cu–O–Si–O– structures can greatly promote the first step, dehydration of glycerol to hydroxyacetone. It should be noted that the exposed surface area of Cu powder is very close to that of 10%Cu/SBA-15(IM) (Table 2). This further confirms that the Cu–O–Si–O– interface structures are responsible for the discrepancy in catalytic activity between Cu powder and 10%Cu/SBA-15(IM). When it comes to 10%Cu/SBA-15(IM) and 10%Cu/SBA-15(G), the peak is much larger in the 1600–1300  $\text{cm}^{-1}$  region for 10%Cu/SBA-15(G). First, more Cu–O–Si–O– structures on 10%Cu/SBA-15(G) give more hydroxyacetone. Second, the exposed copper surface area of 10%Cu/SBA-15(G) is far larger than that of 10%Cu/SBA-15(IM) and the generation of hydroxyacetone can interact with Cu nanoparticles of 10%Cu/SBA-15(G), which facilitates the subsequent hydrogenation step.

To support the above conclusions, Cu powder coated with silica (Cu@SiO<sub>2</sub>) was evaluated in glycerol hydrogenolysis and hydroxyacetone hydrogenation reactions (Table S1). The existence of Cu–O–Si–O– structures in Cu@SiO<sub>2</sub> has been reported by Zheng's group [35]. Besides, it is reported in Section 3.2 that the Cu–O–Si–O– structure is the only source of Lewis acid, so the appearance of Lewis acid sites in Cu@SiO<sub>2</sub> (Fig. S4) clearly demonstrates the formation of the Cu–O–Si–O– structure. As for catalytic performance, glycerol conversion on Cu@SiO<sub>2</sub> (6.5%, Table S1) was about six times that on Cu powder (1.2%, Table S1) in the hydrogenolysis reaction. Glycerol hydrogenolysis and hydroxyacetone hydrogenation reaction results of Cu@SiO<sub>2</sub> (Table S1) again confirmed the crucial role of the Cu–O–Si–O– structure in dehydration. These experimental results indicate that the interfacial Cu–O–Si–O– structures between Cu and SiO<sub>2</sub> (not just SBA-15) could dramatically promote the catalytic activity of Cu/SiO<sub>2</sub> catalysts, irrespective of the type of SiO<sub>2</sub>.

### 3.4. Density functional theory calculation results

As confirmed in Section 3.2, C–OH cleavage in the dehydration step was the rate-determining step of glycerol hydrogenolysis [55,57]. Therefore, investigation of C–OH cleavage can provide a rational interpretation of catalytic behavior for glycerol hydrogenolysis and give information about the active sites for glycerol dehydration.

Because the Cu (1 1 1) surface was the most exposed surface in our experiments, the catalyst model of Cu (1 1 1) was constructed to simulate metallic Cu, while an SiO<sub>2</sub> (1 1 0) surface with an adsorbed Cu<sub>4</sub> cluster structure (Cu<sub>4</sub>/SiO<sub>2</sub>) was built to represent the Cu–O–Si–O– interface. First, the adsorption energy of the most stable structure of glycerol on Cu (1 1 1) and Cu<sub>4</sub>/SiO<sub>2</sub> was investigated (Fig. 8), which is similar to the work reported by

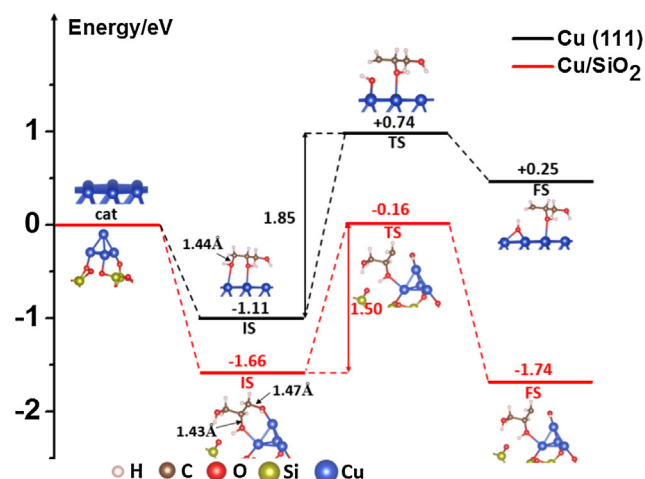


Fig. 8. Energy profile for cleavage of the terminal hydroxyl group of glycerol on Cu (1 1 1) and Cu<sub>4</sub>/SiO<sub>2</sub>. The local configurations of the adsorbates on catalysts at initial states (IS), transition states (TS), and final states (FS) along the minimum-energy pathway are shown in the inserts.

Yun et al. [55]. The adsorption energy of glycerol on Cu (1 1 1) is –1.11 eV, and the terminal C–OH bond is 1.44 Å. For Cu<sub>4</sub>/SiO<sub>2</sub>, the adsorption energy of glycerol is –1.66 eV, and the terminal C–OH bond is 1.47 Å, which is longer than C–OH bonds in glycerol adsorbed onto Cu (1 1 1). The lower  $E_{\text{ads}}$  and longer C–OH bond indicate that the adsorption and activation of glycerol on Cu–O–Si–O– structure is more favorable than Cu surface. We further investigated the energy barrier of terminal C–OH cleavage of glycerol on Cu (1 1 1) and Cu<sub>4</sub>/SiO<sub>2</sub> (Fig. 8). The energy barrier for the removal of terminal hydroxyl group on Cu<sub>4</sub>/SiO<sub>2</sub> is calculated to be 1.50 eV, lower than that on Cu (1 1 1) (1.85 eV). Additionally, the energy barrier for the elimination of center hydroxyl groups was also calculated on Cu<sub>4</sub>/SiO<sub>2</sub> (2.44 eV) and Cu (1 1 1) (2.00 eV), as illustrated in Fig. S8. In both models, the removal of center hydroxyl groups is much more difficult than that of terminal hydroxyl groups, coincidence with the high selectivity to 1,2-PDO (Scheme 1). The energy barrier of hydroxyacetone hydrogenation is 1.20 eV (Fig. S9), which confirms the presumption that C–OH cleavage is the rate-determining step in glycerol hydrogenolysis.

From the above results, we can conclude that the Cu–O–Si–O– interface structures enhance the adsorption of glycerol molecules and lower the energy barrier of terminal hydroxyl group cleavage, which boost the glycerol dehydration step. The DFT calculation results are well consistent with our experimental results that Cu–O–Si–O– interface structures are the primary active sites for glycerol dehydration and can significantly improve the catalytic performance of Cu/SiO<sub>2</sub> catalysts in glycerol hydrogenolysis.

### 3.5. Catalytic stability

Reusability was tested for 10%Cu/SBA-15(G) and 10%Cu/SBA-15(IM) in a third reaction run. After every reaction, the catalyst was separated and dried at 353 K, followed by calcination in air flow at 773 K and reduction under a 10 vol% H<sub>2</sub>/Ar flow at 593 K. Table 5 lists glycerol conversion and 1,2-PDO selectivity in different reaction runs. In the case of 10%Cu/SBA-15(G), glycerol conversion slightly decreased from 59.1% to 52.3% during three catalytic cycles, while 10%Cu/SBA-15(IM) exhibited rather poor stability. After three times of reaction, declines in Cu content (from 9.6% to 7.9%) and Cu exposed surface area (from 5.9 to 3.4  $\text{m}^2_{\text{Cu}} \text{g}_{\text{cat}}^{-1}$ ) could be observed for 10%Cu/SBA-15(IM), but the physicochemical properties of 10%Cu/SBA-15(G) showed no obvious changes. It can be deduced that abundant Cu–O–Si–O– interface structures in

**Table 5**  
Reusability results of glycerol hydrogenolysis over 10%Cu/SBA-15(G) and 10%Cu/SBA-15(IM).

Sample	Glycerol conversion, 1,2-PDO selectivity (%)			$S_{Cu}$ ( $m^2_{Cu} g_{cat}^{-1}$ ) <sup>a</sup>	Cu content (wt.%) <sup>b</sup>
	First run	Second run	Third run		
10%Cu/SBA-15(IM)	8.1, 99.2	4.5, 99.0	2.3, 99.2	3.4	7.9
10%Cu/SBA-15(G)	59.1, 98.7	49.3, 98.3	52.3, 98.8	34.2	9.3

<sup>a</sup> Cu exposed surface area of used catalyst after the third reaction.

<sup>b</sup> Cu content of used catalyst after the third reaction.

10%Cu/SBA-15(G) could not only improve catalytic performance but also stabilize Cu nanoparticles, resulting in superior catalytic activity and stability in glycerol hydrogenolysis.

#### 4. Conclusions

In this work, highly dispersed copper nanoparticles on SBA-15 were fabricated by a simple grinding method. XRD, XPS, and in situ DRIFTS results demonstrated that good dispersion of CuO nanoparticles on calcined 10%Cu/SBA-15(G) resulted from the finely dispersed copper precursor formed by grinding. In the grinding and calcination processes, Cu–O–Si–O– structures were produced in the interface of the nanoscale copper species and SBA-15 surface, and finally worked as anchor sites to stabilize Cu nanoparticles. For the impregnation sample, low dispersion of copper precursor and fewer Cu–O–Si–O– structures resulted in the formation of bulk Cu.

The ground Cu/SBA-15 catalysts with more exposed copper surface area and interfacial Cu–O–Si–O– structures presented excellent catalytic activity and stability in glycerol hydrogenolysis. The conversion of glycerol on 10%Cu/SBA-15(G) was much higher than that of 10%Cu/SBA-15(IM), and both catalysts showed high selectivity to 1,2-PDO above 97%. The TOF of Cu<sup>0</sup> increased linearly with the amount of LAS/Cu<sup>0</sup>, indicating that Lewis acid sites derived from Cu–O–Si–O– structures are a crucial prerequisite for excellent hydrogenolysis performance. More importantly, in situ FT-IR experiments of glycerol adsorption and DFT calculation results evidenced that Cu–O–Si–O– structures were the primary active sites for glycerol dehydration to hydroxyacetone. The hydrogen species adsorbed onto adjacent Cu sites would perform hydroxyacetone hydrogenation smoothly to generate 1,2-PDO.

#### Declaration of Competing Interest

The authors declare that they have no known competing financial interests or personal relationships that could have appeared to influence the work reported in this paper.

#### Acknowledgments

The authors gratefully acknowledge financial support from the National Natural Science Foundation of China (21878321), the Natural Science Foundation of Shanxi Province (2016021033), the Science Foundation for Youth Scholars of the State Key Laboratory of Coal Conversion (2016BWZ002), and the Youth Innovation Promotion Association CAS (2015140). The authors declare that they have no competing interests.

#### Appendix A. Supplementary material

Supplementary data to this article can be found online at <https://doi.org/10.1016/j.jcat.2019.12.032>.

#### References

- [1] A. Corma, S. Iborra, A. Velty, Chemical routes for the transformation of biomass into chemicals, *Chem. Rev.* 107 (2007) 2411–2502.
- [2] D. Sun, Y. Yamada, S. Sato, W. Ueda, Glycerol hydrogenolysis into useful C3 chemicals, *Appl. Catal. B Environ.* 193 (2016) 75–92.
- [3] S. Zhu, X. Gao, Y. Zhu, Y. Zhu, H. Zheng, Y. Li, Promoting effect of boron oxide on Cu/SiO<sub>2</sub> catalyst for glycerol hydrogenolysis to 1,2-propanediol, *J. Catal.* 303 (2013) 70–79.
- [4] C.H. Zhou, J.N. Beltramini, Y.X. Fan, G.Q. Lu, Chemoselective catalytic conversion of glycerol as a biorenewable source to valuable commodity chemicals, *Chem. Soc. Rev.* 37 (2008) 527–549.
- [5] Y. Nakagawa, K. Tomishige, Heterogeneous catalysis of the glycerol hydrogenolysis, *Catal. Sci. Technol.* 1 (2011) 179–190.
- [6] S. Zhu, X. Gao, Y. Zhu, Y. Li, Tailored mesoporous copper/ceria catalysts for the selective hydrogenolysis of biomass-derived glycerol and sugar alcohols, *Green Chem.* 18 (2016) 782–791.
- [7] C. Wang, H. Jiang, C. Chen, R. Chen, W. Xing, Solvent effect on hydrogenolysis of glycerol to 1,2-propanediol over Cu–ZnO catalyst, *Chem. Eng. J.* 264 (2015) 344–350.
- [8] Y. Kang, X. Bu, G. Wang, X. Wang, Q. Li, Y. Feng, A highly active Cu–Pt/SiO<sub>2</sub> bimetal for the hydrogenolysis of glycerol to 1,2-propanediol, *Catal. Lett.* 146 (2016) 1408–1414.
- [9] E.S. Vasiliadou, E. Heracleous, I.A. Vasalos, A.A. Lemonidou, Ru-based catalysts for glycerol hydrogenolysis—effect of support and metal precursor, *Appl. Catal. B Environ.* 92 (2009) 90–99.
- [10] I. Gandarias, J. Requies, P.L. Arias, U. Armbruster, A. Martin, Liquid-phase glycerol hydrogenolysis by formic acid over Ni–Cu/Al<sub>2</sub>O<sub>3</sub> catalysts, *J. Catal.* 290 (2012) 79–89.
- [11] S. Xia, R. Nie, X. Lu, L. Wang, P. Chen, Z. Hou, Hydrogenolysis of glycerol over Cu<sub>0.4</sub>/Zn<sub>5.6</sub>–xMg/Al<sub>2</sub>O<sub>8.6</sub> catalysts: The role of basicity and hydrogen spillover, *J. Catal.* 296 (2012) 1–11.
- [12] J. ten Dam, U. Hanefeld, Renewable chemicals: dehydroxylation of glycerol and polyols, *ChemSusChem* 4 (2011) 1017–1034.
- [13] T. Miyazawa, Y. Kusunoki, K. Kunimori, K. Tomishige, Glycerol conversion in the aqueous solution under hydrogen over Ru/C + an ion-exchange resin and its reaction mechanism, *J. Catal.* 240 (2006) 213–221.
- [14] M. Lee, Y.K. Hwang, J.-S. Chang, H.-J. Chae, D.W. Hwang, Vapor-phase hydrogenolysis of glycerol to 1,2-propanediol using a chromium-free Ni–Cu–SiO<sub>2</sub> nanocomposite catalyst, *Catal. Commun.* 84 (2016) 5–10.
- [15] I. Gandarias, P.L. Arias, J. Requies, M.B. Güemez, J.L.G. Fierro, Hydrogenolysis of glycerol to propanediols over a Pt/ASA catalyst: The role of acid and metal sites on product selectivity and the reaction mechanism, *Appl. Catal. B Environ.* 97 (2010) 248–256.
- [16] I. Furikado, T. Miyazawa, S. Koso, A. Shima, K. Kunimori, K. Tomishige, Catalytic performance of Rh/SiO<sub>2</sub> in glycerol reaction under hydrogen, *Green Chem.* 9 (2007) 582–588.
- [17] F. Auneau, S. Noël, G. Aubert, M. Besson, L. Djakovitch, C. Pinel, On the role of the atmosphere in the catalytic glycerol transformation over iridium-based catalysts, *Catal. Commun.* 16 (2011) 144–149.
- [18] J. Zhou, J. Zhang, X. Guo, J. Mao, S. Zhang, Ag/Al<sub>2</sub>O<sub>3</sub> for glycerol hydrogenolysis to 1,2-propanediol: activity, selectivity and deactivation, *Green Chem.* 14 (2012) 156–163.
- [19] A. Perosa, P. Tundo, Selective hydrogenolysis of glycerol with Raney nickel, *Ind. Eng. Chem. Res.* 44 (2005) 8535–8537.
- [20] X. Guo, Y. Li, W. Song, W. Shen, Glycerol hydrogenolysis over Co catalysts derived from a layered double hydroxide precursor, *Catal. Lett.* 141 (2011) 1458–1463.
- [21] X. Guo, Y. Li, R. Shi, Q. Liu, E. Zhan, W. Shen, Co/MgO catalysts for hydrogenolysis of glycerol to 1, 2-propanediol, *Appl. Catal. A Gen.* 371 (2009) 108–113.
- [22] S. Zhu, X. Gao, Y. Zhu, W. Fan, J. Wang, Y. Li, A highly efficient and robust Cu/SiO<sub>2</sub> catalyst prepared by the ammonia evaporation hydrothermal method for glycerol hydrogenolysis to 1,2-propanediol, *Catal. Sci. Technol.* 5 (2015) 1169–1180.
- [23] P. Hirunsit, C. Luadthong, K. Faungnawakij, Effect of alumina hydroxylation on glycerol hydrogenolysis to 1,2-propanediol over Cu/Al<sub>2</sub>O<sub>3</sub>: combined experiment and DFT investigation, *RSC Adv.* 5 (2015) 11188–11197.
- [24] Z. Yuan, J. Wang, L. Wang, W. Xie, P. Chen, Z. Hou, X. Zheng, Biodiesel derived glycerol hydrogenolysis to 1,2-propanediol on Cu/MgO catalysts, *Bioresour. Technol.* 101 (2010) 7088–7092.

- [25] Z. Yuan, L. Wang, J. Wang, S. Xia, P. Chen, Z. Hou, X. Zheng, Hydrogenolysis of glycerol over homogeneously dispersed copper on solid base catalysts, *Appl. Catal. B Environ.* 101 (2011) 431–440.
- [26] D. Durán-Martín, M. Ojeda, M.L. Granados, J.L.G. Fierro, R. Mariscal, Stability and regeneration of Cu–ZrO<sub>2</sub> catalysts used in glycerol hydrogenolysis to 1,2-propanediol, *Catal. Today* 210 (2013) 98–105.
- [27] M. Balaraju, V. Rekha, P.S.S. Prasad, R.B.N. Prasad, N. Lingaiah, Selective hydrogenolysis of glycerol to 1, 2 Propanediol over Cu–ZnO catalysts, *Catal. Lett.* 126 (2008) 119–124.
- [28] E.S. Vasiliadou, T.M. Eggenhuisen, P. Munnik, P.E. de Jongh, K.P. de Jong, A.A. Lemonidou, Synthesis and performance of highly dispersed Cu/SiO<sub>2</sub> catalysts for the hydrogenolysis of glycerol, *Appl. Catal. B Environ.* 145 (2014) 108–119.
- [29] H. Liu, Z. Huang, Z. Han, K. Ding, H. Liu, C. Xia, J. Chen, Efficient production of methanol and diols via the hydrogenation of cyclic carbonates using copper-silica nanocomposite catalysts, *Green Chem.* 17 (2015) 4281–4290.
- [30] J. Zheng, W. Zhu, C. Ma, Y. Hou, W. Zhang, Z. Wang, Hydrogenolysis of glycerol to 1,2-propanediol on the high dispersed SBA-15 supported copper catalyst prepared by the ion-exchange method, *React. Kinet. Mech. Catal.* 99 (2010) 455–462.
- [31] Y.M. Wang, Z. Ying Wu, J.H. Zhu, Surface functionalization of SBA-15 by the solvent-free method, *J. Solid State Chem.* 177 (2004) 3815–3823.
- [32] Y.M. Wang, Z.Y. Wu, L.Y. Shi, J.H. Zhu, Rapid functionalization of mesoporous materials: directly dispersing metal oxides into as-prepared SBA-15 occluded with template, *Adv. Mater.* 17 (2005) 323–327.
- [33] S. Sato, M. Akiyama, R. Takahashi, T. Hara, K. Inui, M. Yokota, Vapor-phase reaction of polyols over copper catalysts, *Appl. Catal. A Gen.* 347 (2008) 186–191.
- [34] D. Stosic, S. Bennici, S. Sirotnin, P. Stelmachowski, J. Couturier, J. Dubois, A. Travert, A. Auroux, Examination of acid-base properties of solid catalysts for gas phase dehydration of glycerol: FTIR and adsorption microcalorimetry studies, *Catal. Today* 226 (2014) 167–175.
- [35] C. Xu, G. Chen, Y. Zhao, P. Liu, X. Duan, L. Gu, G. Fu, Y. Yuan, N. Zheng, Interfacing with silica boosts the catalysis of copper, *Nat. Commun.* 9 (2018) 3367.
- [36] H. Xi, X. Hou, Y. Liu, S. Qing, Z. Gao, Cu–Al spinel oxide as an efficient catalyst for methanol steam reforming, *Angew. Chem. Int. Ed.* 53 (2014) 11886–11889.
- [37] H. Yang, Y. Chen, X. Cui, G. Wang, Y. Cen, T. Deng, W. Yan, J. Gao, S. Zhu, U. Olsbye, J. Wang, W. Fan, A highly stable copper-based catalyst for clarifying the catalytic roles of Cu<sup>0</sup> and Cu<sup>+</sup> species in methanol dehydrogenation, *Angew. Chem. Int. Ed.* 57 (2018) 1836–1840.
- [38] G. Kresse, J. Furthmuller, Efficiency of ab-initio total energy calculations for metals and semiconductors using a plane-wave basis set, *Comput. Mater. Sci.* 6 (1996) 15–50.
- [39] G. Kresse, J. Furthmuller, Efficient iterative schemes for ab initio total-energy calculations using a plane-wave basis set, *Phys. Rev. B* 54 (1996) 11169–11186.
- [40] P.E. Blöchl, Projector augmented-wave method, *Phys. Rev. B* 50 (1994) 17953–17979.
- [41] G. Kresse, D. Joubert, From ultrasoft pseudopotentials to the projector augmented-wave method, *Phys. Rev. B* 59 (1999) 1758–1775.
- [42] J.P. Perdew, K. Burke, M. Ernzerhof, Generalized gradient approximation made simple, *Phys. Rev. Lett.* 77 (1996) 3865–3868.
- [43] J. Gong, H. Yue, Y. Zhao, S. Zhao, L. Zhao, J. Lv, S. Wang, X. Ma, Synthesis of ethanol via syngas on Cu/SiO<sub>2</sub> catalysts with balanced Cu<sup>0</sup>–Cu<sup>+</sup> sites, *J. Am. Chem. Soc.* 134 (2012) 13922–13925.
- [44] L.F. Chen, P.J. Guo, M.H. Qiao, S.R. Yan, H.X. Li, W. Shen, H.L. Xu, K.N. Fan, Cu/SiO<sub>2</sub> catalysts prepared by the ammonia-evaporation method: Texture, structure, and catalytic performance in hydrogenation of dimethyl oxalate to ethylene glycol, *J. Catal.* 257 (2008) 172–180.
- [45] C.F. Zhou, Y.M. Wang, Y. Cao, T.T. Zhuang, W. Huang, Y. Chun, J.H. Zhu, Solvent-free surface functionalized SBA-15 as a versatile trap of nitrosamines, *J. Mater. Chem.* 16 (2006) 1520–1528.
- [46] Z. Huang, F. Cui, J. Xue, J. Zuo, J. Chen, C. Xia, Cu/SiO<sub>2</sub> catalysts prepared by hom- and heterogeneous deposition-precipitation methods: texture, structure, and catalytic performance in the hydrogenolysis of glycerol to 1,2-propanediol, *Catal. Today* 183 (2012) 42–51.
- [47] A. Yin, X. Guo, W.L. Dai, K. Fan, The nature of active copper species in Cu-HMS catalyst for hydrogenation of dimethyl oxalate to ethylene glycol: new insights on the synergistic effect between Cu<sup>0</sup> and Cu<sup>+</sup>, *J. Phys. Chem. C* 113 (2009) 11003–11013.
- [48] Y. Wang, J. Liao, J. Zhang, S. Wang, Y. Zhao, X. Ma, Hydrogenation of methyl acetate to ethanol by Cu/ZnO catalyst encapsulated in SBA-15, *AlChE J.* 63 (2017) 2839–2849.
- [49] Y.C. Xie, Y.Q. Tang, Spontaneous monolayer dispersion of oxides and salts onto surface of supports: application to heterogeneous catalysis, *Adv. Catal.* 37 (1990) 1–43.
- [50] T. Toupance, M. Kermarec, J.F. Lambert, C. Louis, Conditions of formation of copper phyllosilicates in silica-supported copper catalysts prepared by selective adsorption, *J. Phys. Chem. B* 106 (2002) 2277–2286.
- [51] Z. Huang, H. Liu, F. Cui, J. Zuo, J. Chen, C. Xia, Effects of the precipitation agents and rare earth additives on the structure and catalytic performance in glycerol hydrogenolysis of Cu/SiO<sub>2</sub> catalysts prepared by precipitation-gel method, *Catal. Today* 234 (2014) 223–232.
- [52] Y. Zhu, X. Kong, J. Yin, R. You, B. Zhang, H. Zheng, X. Wen, Y. Zhu, Y. Li, Covalent-bonding to irreducible SiO<sub>2</sub> leads to high-loading and atomically dispersed metal catalysts, *J. Catal.* 353 (2017) 315–324.
- [53] G. Díaz, R. Pérez-Hernández, A. Gómez-Cortés, M. Benaissa, R. Mariscal, J.L.G. Fierro, CuO–SiO<sub>2</sub> Sol-Gel catalysts: characterization and catalytic properties for NO reduction, *J. Catal.* 187 (1999) 1–14.
- [54] J. Ding, T. Popa, J. Tang, K.A.M. Gasem, M. Fan, Q. Zhong, Highly selective and stable Cu/SiO<sub>2</sub> catalysts prepared with a green method for hydrogenation of diethyl oxalate into ethylene glycol, *Appl. Catal. B Environ.* 209 (2017) 530–542.
- [55] Y.S. Yun, T.Y. Kim, D. Yun, K.R. Lee, J.W. Han, J. Yi, Understanding the reaction mechanism of glycerol hydrogenolysis over a CuCr<sub>2</sub>O<sub>4</sub> catalyst, *ChemSusChem* 10 (2016) 442–454.
- [56] E.S. Vasiliadou, A.A. Lemonidou, Kinetic study of liquid-phase glycerol hydrogenolysis over Cu/SiO<sub>2</sub> catalyst, *Chem. Eng. J.* 231 (2013) 103–112.
- [57] Z. Zhou, X. Li, T. Zeng, W. Hong, Z. Cheng, W. Yuan, Kinetics of hydrogenolysis of glycerol to propylene glycol over Cu–ZnO–Al<sub>2</sub>O<sub>3</sub> catalysts, *J. Chin. J. Chem. Eng.* 18 (2010) 384–390.
- [58] J.R. Copeland, G.S. Foo, L.A. Harrison, C. Sievers, In situ ATR-IR study on aqueous phase reforming reactions of glycerol over a Pt/gamma-Al<sub>2</sub>O<sub>3</sub> catalyst, *Catal. Today* 205 (2013) 49–59.
- [59] F. Vila, M. López Granados, R. Mariscal, Significance of isomeric reaction intermediates in the hydrogenolysis of glycerol to 1,2-propanediol with Cu-based catalysts, *Catal. Sci. Technol.* 7 (2017) 3119–3127.
- [60] V.A. Yaylayan, S. Harty-Majors, A.A. Ismail, Monitoring carbonyl-amine reaction and enolization of 1-hydroxy-2-propanone (acetol) by FTIR spectroscopy, *J. Agr. Food Chem.* 47 (1999) 2335–2340.
- [61] M.T. Hernández, M. González, Synthesis of resins as alpha-alumina precursors by the Pechini method using microwave and infrared heating, *J. Eur. Ceram. Soc.* 22 (2002) 2861–2868.